

One-Shot Video Inpainting

Sangjin Lee* Suhwan Cho* Sangyoun Lee

Yonsei University

Abstract

Recently, removing objects from videos and filling in the erased regions using deep video inpainting (VI) algorithms has attracted considerable attention. Usually, a video sequence and object segmentation masks for all frames are required as the input for this task. However, in real-world applications, providing segmentation masks for all frames is quite difficult and inefficient. Therefore, we deal with VI in a one-shot manner, which only takes the initial frame’s object mask as its input. Although we can achieve that using naive combinations of video object segmentation (VOS) and VI methods, they are sub-optimal and generally cause critical errors. To address that, we propose a unified pipeline for one-shot video inpainting (OSVI). By jointly learning mask prediction and video completion in an end-to-end manner, the results can be optimal for the entire task instead of each separate module. Additionally, unlike the two-stage methods that use the predicted masks as ground truth cues, our method is more reliable because the predicted masks can be used as the network’s internal guidance. On the synthesized datasets for OSVI, our proposed method outperforms all others both quantitatively and qualitatively.

1 Introduction

Video inpainting (VI) is a task that aims to remove a designated object in a given video sequence and fill in that area with plausible content. General approaches for VI take a video sequence and object segmentation masks for all frames as their input. However, in real-world applications, obtaining object segmentation masks for every frame is usually difficult and labor-intensive. To address this issue, we expand on an approach that is better suited to practical scenarios, namely one-shot video inpainting (OSVI). Compared to a conventional VI that requires full-frame segmentation masks as shown in Figure 1 (a), OSVI requires only the initial frames’s object mask and internally predicts those of subsequent frames while filling the missing content for all frames; this is depicted in Figure 1 (b).

OSVI can be achieved by sequentially connecting a video object segmentation (VOS) network and a VI network as a two-stage pipeline. Using the initial frame object annotation, the VOS network first generates that object’s entire

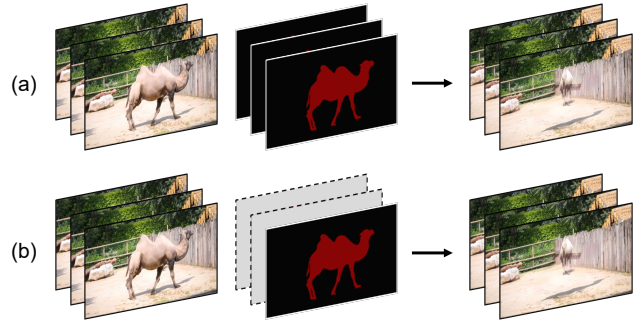


Figure 1: Visualized comparison between the definitions of (a) conventional video inpainting and (b) one-shot video inpainting.

frame masks. Then, using full-frame object masks as its input, the VI network fills in the object regions with plausible content that befits the background. However, this two-stage approach suffers from critical issues when directly applied to OSVI. Here, we will discuss this approach’s two main problems. First, since the entire network is not trained in an end-to-end manner, the results are optimal for each separate module but not as a whole. This property that two different networks are trained based on respective objectives leads to sub-optimal results for OSVI. Second, existing VI algorithms assume that the object masks received as input are always accurate. Therefore, if the predicted masks generated from a VOS model, which could be inaccurate, are provided as their input, the system will severely break down. This phenomenon will be particularly more drastic for flow-based VI methods where reference pixels are directly warped to the target region.

To address these concerns, we propose an end-to-end learnable baseline network that consists of mask prediction and video completion modules sharing a single encoder’s embedded features. Unlike existing VI algorithms, we erase the object region at the feature level by adopting a novel transformer architecture. Our proposed method demonstrates its effectiveness for OSVI on synthetic datasets both quantitatively and qualitatively. Compared with two-stage methods, which are mainly naive combinations of existing VOS and VI methods, our method surpasses all of them by

*These authors contributed equally.

a large margin.

Our main contributions can be summarized as follows:

- We expand VI to OSVI, which refers to erasing a designated object in a video sequence only using a single frame annotation.
- We propose a novel end-to-end learnable algorithm that can handle OSVI more effectively when compared to existing two-stage approaches.
- Our proposed method outperforms all existing methods on synthetic datasets.

2 Related Work

Object removal. Due to its usefulness in diverse vision applications, such as video editing, object removal has been of interest recently. Shetty *et al.* (Shetty, Fritz, and Schiele 2018) propose a GAN-based two-stage network composed of a mask generator and an image inpainter for object removal in an image. DynaFill (Bešić and Valada 2020) presents a new type of network using depth completion on the inpainted image. The depth map predicted from the inpainted image of a previous frame is used as guidance for current frame image inpainting. AutoRemover (Zhang *et al.* 2020) takes masks as its input and detects shadows using them. By using object masks and extracted shadow masks, the network can erase their shadows as well as objects in a video. VORNet (Chang, Yu Liu, and Hsu 2019) fills the missing object regions only with box annotations as weak supervision to reduce annotation efforts.

Video object segmentation. Semi-supervised VOS is a pixel-level classification task that tracks and segments an arbitrary target object in a video. To efficiently handle an arbitrary target object, early works, such as OSVOS (Caelles *et al.* 2017), OnAVOS (Voigtlaender and Leibe 2017) and OSVOS-S (Maninis *et al.* 2018), are based on online learning that trains a network during test time. However, since online learning is impractical for real-world applications because of its huge computational cost at test time, recent methods are based on feature matching that compares query frame features to reference frame features without online learning. VideoMatch (Hu, Huang, and Schwing 2018) extracts features from an initial frame and a query frame and then matches them at pixel-level using a soft matching layer. FEELVOS (Voigtlaender *et al.* 2019) extends the use of pixel-level matching by employing initial and previous frames as reference ones; it also uses the matching output as the network’s internal guidance. CFBI (Yang, Wei, and Yang 2020) improves FEELVOS by employing background matching as well as foreground matching. To fully utilize the information from all past frames as well as initial and previous frames, STM (Oh *et al.* 2019a) proposes the space–time memory network, in which query frame features are densely matched to the memory features built from all past frames, covering all space–time locations. AFB-URR (Liang *et al.* 2020) and XMem (Cheng and Schwing 2022) improves the memory construction scheme to design a model robust to long videos.

Video inpainting. Early works (Huang *et al.* 2016; Wexler, Shechtman, and Irani 2004) use patch-based optimization

to restore missing regions with valid regions for VI. However, these methods have some limitations. For example, they face difficulty in representing dynamic motions while maintaining temporal consistency, in addition to requiring high computational costs. To address these issues, various deep learning-based methods have been proposed within the past few years. These studies can be divided into two categories: patch-based approaches (Lee *et al.* 2019; Oh *et al.* 2019b; Zeng, Fu, and Chao 2020; Li *et al.* 2020; Liu *et al.* 2021) and flow-based approaches (Kim *et al.* 2019; Xu *et al.* 2019; Gao *et al.* 2020; Zou *et al.* 2021; Li *et al.* 2022). Patch-based approaches aim to fill missing regions using direct pixel-level feature matching. CPNet (Lee *et al.* 2019) uses an alignment network to fill missing regions by using the different object positions with background matching. OPN (Oh *et al.* 2019b) proposes a similarity matching network that extracts and compares key and value features for each frame. It also suggests a post-processing network called the TCN, which uses a recurrent structure to increase temporal consistency. STTN (Zeng, Fu, and Chao 2020) is composed of an encoder–decoder architecture and multi-layer multi-head spatio-temporal transformers trained using a 3D discriminator for temporal consistency. BSCA (Li *et al.* 2020) proposes a boundary-aware short-term module for adjacent frame matching and a dynamic long-term context aggregation module for temporal consistency. FuseFormer (Liu *et al.* 2021) develops the transformer-based algorithms by proposing a method of efficiency patch splitting and composing. By contrast, flow-based approaches exploit the optical flow map for VI. VINet (Kim *et al.* 2019) proposes a flow warping-based recurrent network that refers to adjacent frames. DFVI (Xu *et al.* 2019) restores flow maps extracted using a pre-trained flow estimation network by performing forward–backward pixel propagation. FGVC (Gao *et al.* 2020) presents a flow–edge completion technique for the sharpness of flow map edges, a color propagation in the gradient domain for reducing warping error, and a non-local flow to resolve the chronic problem of flow maps; the latter namely being that they cannot obtain clearness when adjacent frames lack in information. TSAM (Zou *et al.* 2021) proposes a method that applies flow warping to the feature level based on the DNN architecture. E2FGVI (Li *et al.* 2022) shows the problems of previous flow-based pipelines and solves them by presenting the unified pipeline in an end-to-end manner.

3 Proposed Approach

3.1 Problem Formulation

Let us denote a video as $I := \{I^i \in [0, 255]^{3 \times H_0 \times W_0} \mid i = 0, 1, \dots, T-1\}$, ground truth object masks as $M := \{M^i \in \{0, 1\}^{H_0 \times W_0} \mid i = 0, 1, \dots, T-1\}$, and a ground truth clean video as $O := \{O^i \in [0, 255]^{3 \times H_0 \times W_0} \mid i = 0, 1, \dots, T-1\}$. Our goal is to generate the predicted object masks \hat{M} and clean video \hat{O} , where I and M^0 are provided as input.

3.2 Network Overview

An overview of our proposed network is shown in Figure 2. It consists of two modules, a mask prediction module and a

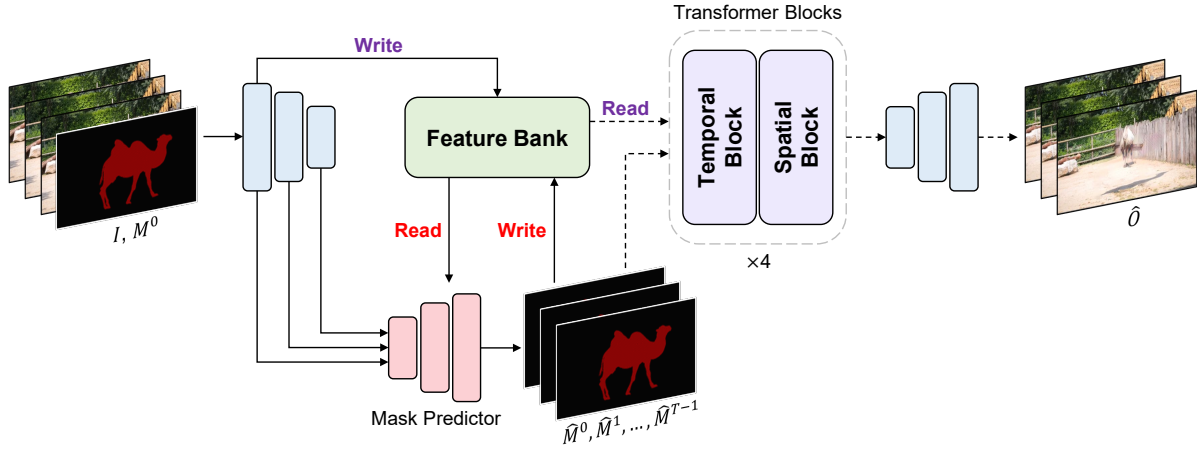


Figure 2: Overall architecture of our proposed algorithm. Solid lines indicate an operation is performed every frame, and dotted lines indicate an operation is performed after all solid line operations are done. Dotted lined operation takes a full-frame information as its input and generates full-frame predictions as its output at once. Red and purple letters refer to the information flows of the mask prediction and video completion, respectively.

video completion module. First, the mask prediction module predicts the segmentation masks for all frames using the segmentation mask from the initial frame and the features extracted from each frame. The predicted masks and the extracted features are stored in a feature bank for reuse. As the semantic cues obtained from the mask prediction module are transferred to the video completion module without gradient disconnection, the entire network can be trained in an end-to-end manner.

3.3 Mask Prediction Module

Memory construction. To propagate the object information of the initial frame, i.e., ground truth segmentation mask, we employ a memory-based architecture as in STM (Oh et al. 2019a). From I^0 , we first extract base features X^0 . Then, key features $K^0 \in \mathbb{R}^{C_K \times HW}$ and value features $V^0 \in \mathbb{R}^{C_V \times HW}$ can be obtained as

$$K^0 = \text{Conv}(X^0), \quad (1)$$

$$V^0 = \text{Conv}(X^0 \oplus \text{down}(M^0)), \quad (2)$$

where \oplus and *down* indicate channel concatenation and adaptive spatial pooling, respectively. The extracted key and value features are then stored in memory to be used for future frame prediction.

One of the memory architecture’s main advantages is its ability to simultaneously store an arbitrary number of frames in memory. To fully exploit dense cues of a video, we store the key and value features of every five frames in the memory as well as the initial frame during the inference. Assuming N frames are stored in the memory, the memory key and value features can be defined as $K_M \in \mathbb{R}^{C_K \times NHW}$ and $V_M \in \mathbb{R}^{C_V \times NHW}$, respectively.

Memory read. Based on the accumulated information (memory key and value features) obtained from past frames, the goal is to predict the query frame mask. To this end, we first extract query key features $K_Q \in \mathbb{R}^{C_K \times HW}$ from the

query frame image and compare them to memory key features K_M to calculate visual similarity. Then, we transfer the object cues, i.e., the memory value features V_M , to the query frame and the query frame value features $V_Q \in \mathbb{R}^{C_V \times HW}$ can be obtained. This process is identical to popular self-attention mechanism (Vaswani et al. 2017), and can be represented as

$$\text{sim} = \text{Softmax}(K_M^T \otimes K_Q), \quad (3)$$

$$V_Q = V_M \otimes \text{sim}, \quad (4)$$

where *Softmax* and \otimes indicate a query-wise softmax operation and matrix multiplication.

Mask prediction. As V_Q contains object cues of the query frame, object segmentation masks \hat{M} can be obtained by decoding it. To do that, we gradually increase the spatial size using the low-level features extracted from the encoder via skip connections. To obtain better feature representations, we add a CBAM (Woo et al. 2018) layer after every skip connection.

3.4 Video Completion Module

Masked multi-head attention. In our framework, visual features are extracted from a video sequence and stored in the feature bank to be used for both mask prediction and video completion modules. Unlike conventional VI methods where object features are excluded, the features in our model contain object information since they should also be used to track a designated object. Considering object features may be referenced when filling the missing region, this will severely degrade the performance of the system. To address this issue, we propose a novel masked multi-head attention (MMHA) for transformer architecture.

The MMHA’s visualized workflow is shown in Figure 3 (a). Given that F represents input features of a transformer block and \hat{m} is a downsampled version of \hat{M} , we can obtain a mask guidance matrix $G \in [0, 1]^{TH'W' \times TH'W'}$ as

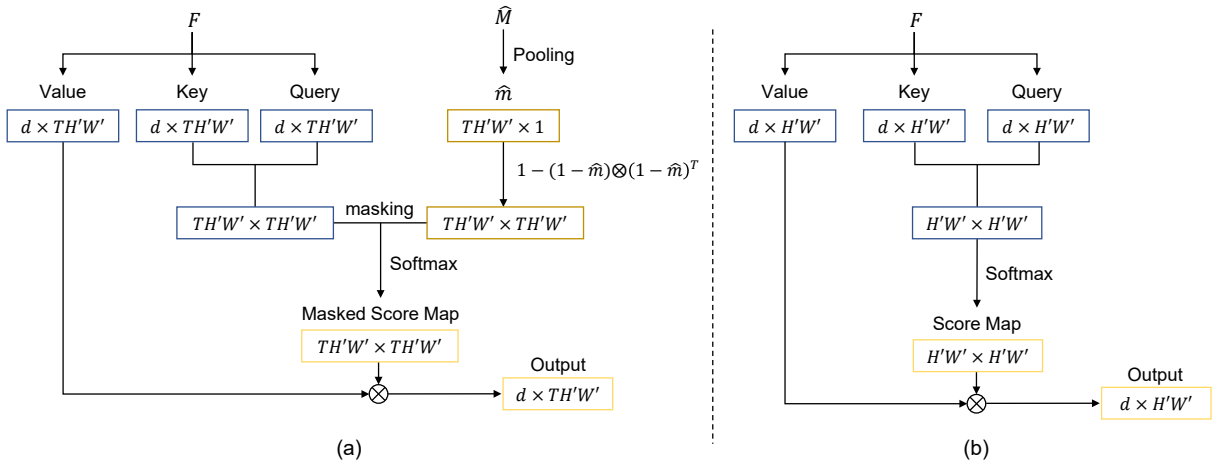


Figure 3: Visualized pipelines of (a) masked multi-head attention and (b) spatial multi-head attention.

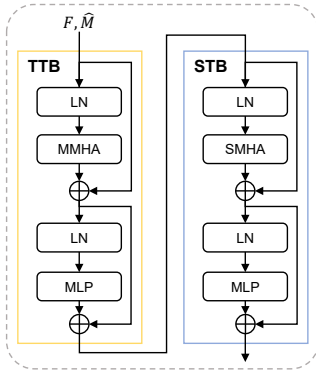


Figure 4: Architecture of our transformer block.

$1 - (1 - \hat{m}) \otimes (1 - \hat{m})^T$, after reshaping \hat{m} to $TH'W' \times 1$. Then, the mask guidance matrix is masked to a key–query similarity map to remove the object region from consideration. However, as a softmax operation comes after this process, we adopt a value substitution operation instead of a simple multiplication. This process can be represented as

$$masking(s, G) = \begin{cases} -\infty & G < 0.5 \\ s & otherwise, \end{cases} \quad (5)$$

where $s \in \mathbb{R}^{TH'W' \times TH'W'}$ indicates the key–query matching scores. This allows us to diminish the influence of the object regions even after the softmax operation. In summary, the MMHA plays two roles: 1) it prevents object regions from bringing semantic cues from other object regions; 2) it forces object regions not to affect other valid regions by limiting content propagation.

Spatio-temporal transformer. As shown in Figure 4, we divide the general transformer block into a temporal transformer block (TTB) and a spatial transformer block (STB). The architectures of both are identical to that of the general transformer architecture, i.e., the sequential connection of multi-head attention and multi-layer perceptron. However,

the TTB exchanges semantic cues between multiple frames, while the STB internally exchanges semantic cues in a single frame. Furthermore, due to the difference in the attention layer, they have different objectives. The TTB is used to erase object cues and fill object regions by leveraging the cues from other frames, while the STB is used to internally fill those regions within a single frame.

Given that F_l is l -th features where $l \in \{0, 1, \dots, L - 1\}$, and L is the number of total transformer blocks, the transformer block formula can be defined as

$$F'_l = \text{MMHA}(\text{LN}(F_l), \hat{M}) + F_l, \quad (6)$$

$$\hat{F}_l = \text{MLP}(\text{LN}(F'_l)) + F'_l, \quad (7)$$

$$F''_l = \text{SMHA}(\text{LN}(\hat{F}_l)) + \hat{F}_l, \quad (8)$$

$$F_{l+1} = \text{MLP}(\text{LN}(F''_l)) + F''_l, \quad (9)$$

where MLP and LN indicate multi-layer perceptron and layer normalization layer (Ba, Kiros, and Hinton 2016), respectively.

3.5 Loss Function

To learn the mask prediction module, we apply mask loss for network training. It is a standard cross-entropy loss, as described in Eqn. 10, where p indicates a single pixel location in M .

$$L_{mask} = - \sum_p \log P(\hat{M} = M) \quad (10)$$

For the video completion module, we use L_1 loss by separately applying it to the object and valid regions. We weight the loss based on the number of pixels in the area as each video has different ratios of object and valid regions. The losses are defined as

$$L_{object} = \frac{\|M \odot (\hat{O} - O)\|_1}{\|M\|_1}, \quad (11)$$

$$L_{valid} = \frac{\|(1 - M) \odot (\hat{O} - O)\|_1}{\|1 - M\|_1}, \quad (12)$$

Table 1: Quantitative evaluation on the synthesized datasets.

VOS	VI	DAYT			BLDA		
		PSNR \uparrow	SSIM \uparrow	LPIPS \downarrow	PSNR \uparrow	SSIM \uparrow	LPIPS \downarrow
FRTM	CPNet	27.038	0.9324	0.0946	29.998	0.9644	0.0451
	STTN	25.357	0.9118	0.1032	28.167	0.9388	0.0552
	FGVC	27.082	0.9300	0.0922	30.114	0.9650	0.0409
	FuseFormer	28.495	0.9343	0.0901	34.115	0.9661	0.0422
CFBI	CPNet	31.985	0.9591	0.0616	33.716	0.9728	0.0336
	STTN	30.388	0.9400	0.0618	31.139	0.9477	0.0414
	FGVC	32.124	0.9541	0.0484	34.491	0.9749	0.0240
	FuseFormer	<u>34.309</u>	<u>0.9623</u>	0.0472	38.427	0.9751	0.0282
BMVOS	CPNet	31.910	0.9587	0.0596	33.405	0.9723	0.0325
	STTN	30.173	0.9389	0.0615	30.799	0.9464	0.0420
	FGVC	31.941	0.9523	0.0487	33.719	0.9737	0.0248
	FuseFormer	34.055	0.9607	0.0480	36.679	0.9742	0.0289
TBD	CPNet	32.479	0.9597	0.0585	35.202	0.9755	0.0274
	STTN	30.469	0.9405	0.0600	32.021	0.9502	0.0362
	FGVC	32.105	0.9533	0.0490	35.247	0.9766	0.0202
	FuseFormer	34.296	0.9618	<u>0.0479</u>	<u>38.785</u>	<u>0.9771</u>	0.0246
Ours		35.518	0.9650	0.0515	38.959	0.9783	0.0268

where \odot indicates Hadamard product. To ensure high perceptual quality, we also employ adversarial loss. The discriminator D takes O and \hat{O} as its input, and outputs 1 if input seems real and 0 if input seems fake. By contrary, the network is trained make the discriminator make a wrong decision by generating a real-like fake image. The loss function for the discriminator is formulated as

$$L_{dis} = \mathbb{E}_O[\log D(O)] + \mathbb{E}_{\hat{O}}[\log(1 - D(\hat{O}))], \quad (13)$$

where the loss function for the network is formulated as

$$L_{adv} = \mathbb{E}_{\hat{O}}[\log D(\hat{O})]. \quad (14)$$

In conclusion, total loss for our network can be defined as follows.

$$L_{total} = L_{mask} + L_{object} + L_{valid} + L_{adv} \quad (15)$$

3.6 Network Training

We adopt two datasets for network training, COCO (Lin et al. 2014) and YouTube-VOS 2018 (Xu et al. 2018). As COCO is an image dataset, we randomly augment each image to generate videos, following the protocol in STM (Oh et al. 2019a) and TBD (Cho et al. 2022b). We resize all training videos to a 240×432 resolution and use them as clean videos. To generate input videos, we attach objects scrapped from other training snippets. The batch size is set to four and each snippet contains seven frames. We use an Adam optimizer (Kingma and Ba 2014) for network optimization.

4 Experiments

4.1 Experimental Setup

Datasets. To validate the effectiveness of our method, we synthesize the testing videos using DAVIS (Perazzi et al.

2016; Pont-Tuset et al. 2017), YouTube-VOS 2018 (Xu et al. 2018), and BL30K (Cheng, Tai, and Tang 2021) datasets. We design two synthesized datasets, DAYT and BLDA, which mean DAVIS objects on YouTube-VOS 2018 videos and BL30K objects on DAVIS videos. DAYT and BLDA consist of 88 and 120 video sequences, each consisting of input images, object masks, and output clean images.

Detailed settings. To compare our method with existing two-stage methods, we use state-of-the-art VI and VOS methods with publicly available pre-trained models. As DAVIS and BL30K are used to construct objects in our testing datasets, we do not adopt VOS models trained on those datasets. For a fair comparison, we use the official code and pre-trained models for all methods. All experiments are implemented on a single RTX A6000 GPU.

4.2 Quantitative Results

We quantitatively compare our method to existing two-stage methods in Table 1. For the VOS models, we adopt FRTM (Robinson et al. 2020), CFBI (Yang, Wei, and Yang 2020), BMVOS (Cho et al. 2022a), and TBD (Cho et al. 2022b). For the VI models, CPNet (Lee et al. 2019), STTN (Zeng, Fu, and Chao 2020), FGVC (Gao et al. 2020), and FuseFormer (Liu et al. 2021) are used. Among the VI models, FuseFormer shows the highest performance. When compared to other two-stage methods, it obtains the best accuracy on DAYT with CFBI, and on BLDA with TBD. We can also observe that if segmentation masks are not accurate enough, satisfactory OSVI performance cannot be achieved even if the state-of-the-art VI method is adopted. This supports the claim that a unified OSVI pipeline capable of effectively handling such noises or errors is needed. On both datasets, our method significantly outperforms all



Figure 5: Qualitative comparison between state-of-the-art two-stage methods and our proposed method. Green regions indicate the object regions to be removed.

Table 2: Ablation study on our proposed algorithm on the synthesized datasets.

Version	PSNR \uparrow	DAYT SSIM \uparrow	LPIPS \downarrow	PSNR \uparrow	BLDA SSIM \uparrow	LPIPS \downarrow
w/o mask loss	24.624	0.9247	0.1075	28.218	0.9561	0.0589
w/o mask guidance	33.298	0.9558	0.0638	36.713	0.9719	0.0353
SMHA \rightarrow MMHA	26.970	0.9287	0.0955	29.647	0.9580	0.0529
no end-to-end training	34.871	0.9633	0.0539	37.292	0.9762	0.0304
w/o encoder sharing	32.324	0.9526	0.0694	35.790	0.9703	0.0375
Ours	35.518	0.9650	0.0515	38.959	0.9783	0.0268

previous methods in PSNR and SSIM metrics. Quantitative results demonstrate the superiority of our method compared to state-of-the-art two-stage methods.

4.3 Qualitative Results

In Figure 5 and Figure 6, we qualitatively compare our method to state-of-the-art two-stage methods. As a VOS model, TBD (Cho et al. 2022b) is adopted for all VI models because it quantitatively outperforms other methods in Table 1. From Figure 5, we can conclude that optical flow-based methods, such as FGVC (Gao et al. 2020), are inadequate for OSVI. This is because un-erased objects may be copied and pasted to fill the object regions, and make the flow-based method produce the artifacts or some afterimages. Our method shows the clearest and most accurate object removal quality. Qualitative results are also compared in video form in Figure 6.

4.4 Ablation Study

In Table 2, we conduct an ablation study on various components of our method. Each different version is quantitatively compared on two synthesized datasets, DAYT and BLDA.

Mask loss. We conduct a study on the use of mask loss

to figure out how mask supervision affects object removal quality. Removing mask loss leads to a drastic performance degradation as small errors in object regions lead to critical errors in the entire system. This demonstrates the need for mask supervision via mask loss is an essential component.

Mask guidance. To filter out object cues extracted from the feature encoder, we apply the mask guidance matrix in MMHA. The quantitative results demonstrate the effectiveness of this filtering process. Compared to the model version without filtering, the model version with filtering shows better performance on all metrics.

Multi-head attention. As TTB focuses on filling the object regions missing the object cues, we utilize STB to focus on filling the object regions that cannot be filled in TTB. Therefore, we apply the MMHA method only to TTB and not to STB. To prove its functionality, we evaluate the model version designed with MMHA instead of SMHA. It turns out that the employed masked attention was ineffective, in which it could not fill the object regions. Thus, the collaborative employment of masked attention for temporal information and naive attention for spatial information is required for OSVI.

End-to-end training. To demonstrate the effectiveness of

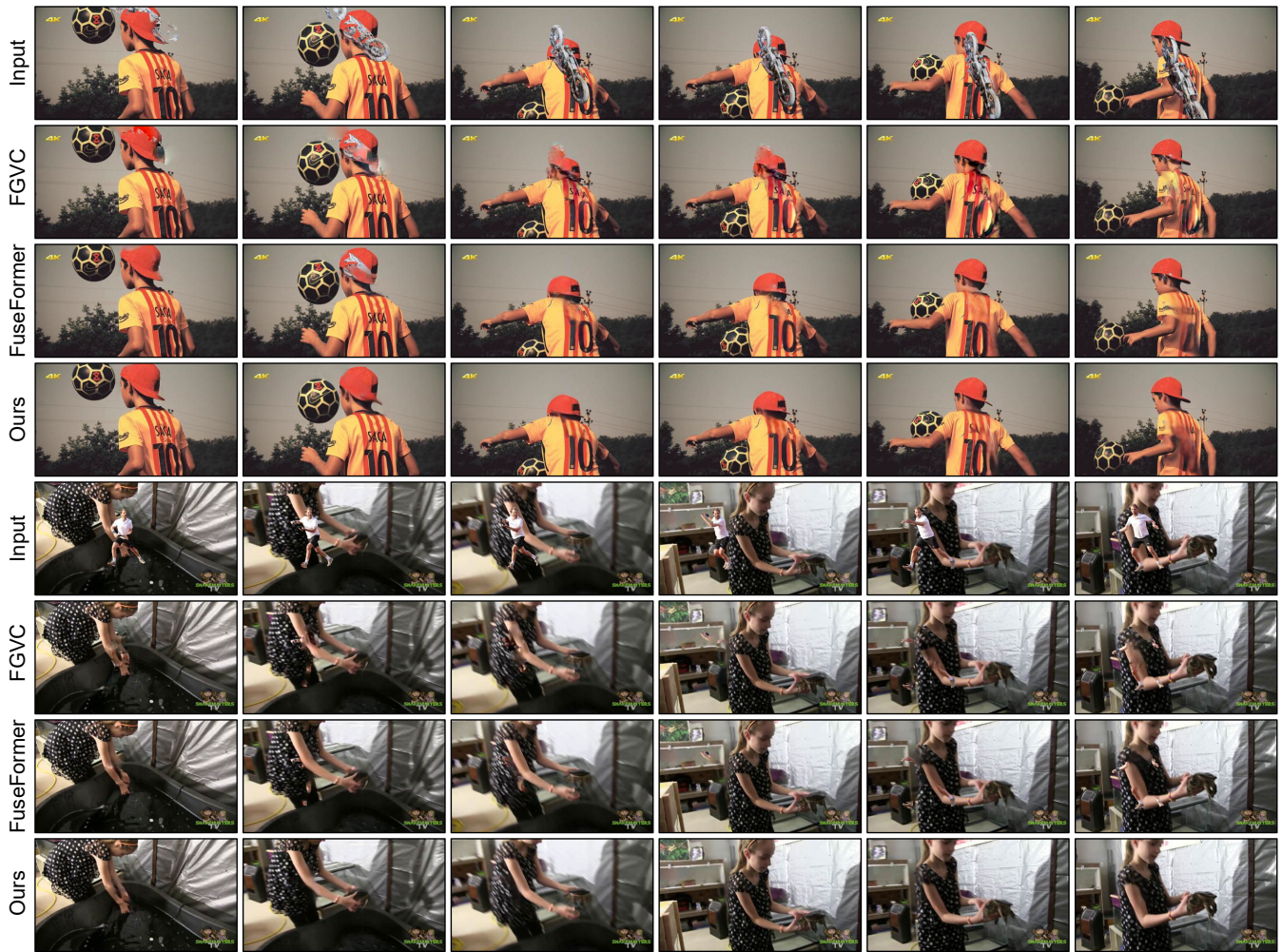


Figure 6: Example input and output videos of different one-shot video inpainting algorithms.

end-to-end network training, we compare the models with and without the end-to-end training protocol. For the model without end-to-end training, the video completion module takes ground truth masks and extracted features without gradients to be separately trained from the mask prediction module. As observed from the table, end-to-end network training enables the network to be more effective. Meaningful improvements are observable for all metrics.

Encoder sharing. We also conduct an experiment to see the difference between models with single and multiple encoders. It is interesting to observe that using a single encoder shows much better performance than using separate encoders. This demonstrates that mask prediction and video completion share common complementary properties. Moreover, jointly learning them ensures a more appropriate network for OSVI.

5 Conclusion

Inspired by inefficiency of conventional VI methods for real-world applications, we deal with the task of OSVI only re-

quiring a single-frame manual annotation. To better deal with this without merely sequentially connecting existing VOS and VI algorithms, we propose an end-to-end learnable baseline model. By a significant margin, our method outperforms all existing two-stage methods both quantitatively and qualitatively on two synthesized datasets. We believe our research makes a step towards efficient and applicable VI.

References

- Ba, J. L.; Kiros, J. R.; and Hinton, G. E. 2016. Layer normalization. *arXiv preprint arXiv:1607.06450*.
- Bešić, B.; and Valada, A. 2020. Dynamic Object Removal and Spatio-Temporal RGB-D Inpainting via Geometry-Aware Adversarial Learning. *arXiv preprint arXiv:2008.05058*.
- Caelles, S.; Maninis, K.-K.; Pont-Tuset, J.; Leal-Taixé, L.; Cremers, D.; and Van Gool, L. 2017. One-shot video object segmentation. In *Proceedings of the IEEE conference on computer vision and pattern recognition*, 221–230.
- Chang, Y.-L.; Yu Liu, Z.; and Hsu, W. 2019. Vornet: Spatio-

- temporally consistent video inpainting for object removal. In *Proceedings of the IEEE/CVF Conference on Computer Vision and Pattern Recognition Workshops*, 0–0.
- Cheng, H. K.; and Schwing, A. G. 2022. XMem: Long-Term Video Object Segmentation with an Atkinson-Shiffrin Memory Model. *arXiv preprint arXiv:2207.07115*.
- Cheng, H. K.; Tai, Y.-W.; and Tang, C.-K. 2021. Modular Interactive Video Segmentation: Interaction-to-Mask, Propagation and Difference-Aware Fusion. In *CVPR*.
- Cho, S.; Lee, H.; Kim, M.; Jang, S.; and Lee, S. 2022a. Pixel-Level Bijective Matching for Video Object Segmentation. In *Proceedings of the IEEE/CVF Winter Conference on Applications of Computer Vision*, 129–138.
- Cho, S.; Lee, H.; Lee, M.; Park, C.; Jang, S.; Kim, M.; and Lee, S. 2022b. Tackling Background Distraction in Video Object Segmentation. *arXiv preprint arXiv:2207.06953*.
- Gao, C.; Saraf, A.; Huang, J.-B.; and Kopf, J. 2020. Flow-edge guided video completion. In *European Conference on Computer Vision*, 713–729. Springer.
- Hu, Y.-T.; Huang, J.-B.; and Schwing, A. G. 2018. Video-match: Matching based video object segmentation. In *Proceedings of the European Conference on Computer Vision (ECCV)*, 54–70.
- Huang, J.-B.; Kang, S. B.; Ahuja, N.; and Kopf, J. 2016. Temporally coherent completion of dynamic video. *ACM Transactions on Graphics (TOG)*, 35(6): 1–11.
- Kim, D.; Woo, S.; Lee, J.-Y.; and Kweon, I. S. 2019. Deep video inpainting. In *Proceedings of the IEEE/CVF Conference on Computer Vision and Pattern Recognition*, 5792–5801.
- Kingma, D. P.; and Ba, J. 2014. Adam: A method for stochastic optimization. *arXiv preprint arXiv:1412.6980*.
- Lee, S.; Oh, S. W.; Won, D.; and Kim, S. J. 2019. Copy-and-paste networks for deep video inpainting. In *Proceedings of the IEEE/CVF International Conference on Computer Vision*, 4413–4421.
- Li, A.; Zhao, S.; Ma, X.; Gong, M.; Qi, J.; Zhang, R.; Tao, D.; and Kotagiri, R. 2020. Short-Term and Long-Term Context Aggregation Network for Video Inpainting. In *European Conference on Computer Vision*, 728–743. Springer.
- Li, Z.; Lu, C.-Z.; Qin, J.; Guo, C.-L.; and Cheng, M.-M. 2022. Towards an end-to-end framework for flow-guided video inpainting. In *Proceedings of the IEEE/CVF Conference on Computer Vision and Pattern Recognition*, 17562–17571.
- Liang, Y.; Li, X.; Jafari, N.; and Chen, J. 2020. Video object segmentation with adaptive feature bank and uncertain-region refinement. *Advances in Neural Information Processing Systems*, 33: 3430–3441.
- Lin, T.-Y.; Maire, M.; Belongie, S.; Hays, J.; Perona, P.; Ramanan, D.; Dollár, P.; and Zitnick, C. L. 2014. Microsoft coco: Common objects in context. In *European conference on computer vision*, 740–755. Springer.
- Liu, R.; Deng, H.; Huang, Y.; Shi, X.; Lu, L.; Sun, W.; Wang, X.; Dai, J.; and Li, H. 2021. Fuseformer: Fusing fine-grained information in transformers for video inpainting. In *Proceedings of the IEEE/CVF International Conference on Computer Vision*, 14040–14049.
- Maninis, K.-K.; Caelles, S.; Chen, Y.; Pont-Tuset, J.; Leal-Taixé, L.; Cremers, D.; and Van Gool, L. 2018. Video object segmentation without temporal information. *IEEE transactions on pattern analysis and machine intelligence*, 41(6): 1515–1530.
- Oh, S. W.; Lee, J.-Y.; Xu, N.; and Kim, S. J. 2019a. Video object segmentation using space-time memory networks. In *Proceedings of the IEEE International Conference on Computer Vision*, 9226–9235.
- Oh, S. W.; Lee, S.; Lee, J.-Y.; and Kim, S. J. 2019b. Onion-peel networks for deep video completion. In *Proceedings of the IEEE/CVF International Conference on Computer Vision*, 4403–4412.
- Perazzi, F.; Pont-Tuset, J.; McWilliams, B.; Van Gool, L.; Gross, M.; and Sorkine-Hornung, A. 2016. A Benchmark Dataset and Evaluation Methodology for Video Object Segmentation. In *Computer Vision and Pattern Recognition*.
- Pont-Tuset, J.; Perazzi, F.; Caelles, S.; Arbeláez, P.; Sorkine-Hornung, A.; and Van Gool, L. 2017. The 2017 DAVIS Challenge on Video Object Segmentation. *arXiv:1704.00675*.
- Robinson, A.; Lawin, F. J.; Danelljan, M.; Khan, F. S.; and Felsberg, M. 2020. Learning Fast and Robust Target Models for Video Object Segmentation. In *IEEE/CVF Conference on Computer Vision and Pattern Recognition (CVPR)*.
- Shetty, R.; Fritz, M.; and Schiele, B. 2018. Adversarial scene editing: Automatic object removal from weak supervision. *arXiv preprint arXiv:1806.01911*.
- Vaswani, A.; Shazeer, N.; Parmar, N.; Uszkoreit, J.; Jones, L.; Gomez, A. N.; Kaiser, Ł.; and Polosukhin, I. 2017. Attention is all you need. *Advances in neural information processing systems*, 30.
- Voigtlaender, P.; Chai, Y.; Schroff, F.; Adam, H.; Leibe, B.; and Chen, L.-C. 2019. Feelvos: Fast end-to-end embedding learning for video object segmentation. In *Proceedings of the IEEE Conference on Computer Vision and Pattern Recognition*, 9481–9490.
- Voigtlaender, P.; and Leibe, B. 2017. Online adaptation of convolutional neural networks for the 2017 davis challenge on video object segmentation. In *The 2017 DAVIS Challenge on Video Object Segmentation-CVPR Workshops*, volume 5.
- Wexler, Y.; Shechtman, E.; and Irani, M. 2004. Space-time video completion. In *Proceedings of the 2004 IEEE Computer Society Conference on Computer Vision and Pattern Recognition, 2004. CVPR 2004.*, volume 1, I–I. IEEE.
- Woo, S.; Park, J.; Lee, J.-Y.; and Kweon, I. S. 2018. Cbam: Convolutional block attention module. In *Proceedings of the European conference on computer vision (ECCV)*, 3–19.
- Xu, N.; Yang, L.; Fan, Y.; Yue, D.; Liang, Y.; Yang, J.; and Huang, T. 2018. Youtube-vos: A large-scale video object segmentation benchmark. *arXiv preprint arXiv:1809.03327*.
- Xu, R.; Li, X.; Zhou, B.; and Loy, C. C. 2019. Deep flow-guided video inpainting. In *Proceedings of the IEEE/CVF Conference on Computer Vision and Pattern Recognition*, 3723–3732.

Yang, Z.; Wei, Y.; and Yang, Y. 2020. Collaborative video object segmentation by foreground-background integration. *arXiv preprint arXiv:2003.08333*.

Zeng, Y.; Fu, J.; and Chao, H. 2020. Learning Joint Spatial-Temporal Transformations for Video Inpainting. In *European Conference on Computer Vision*, 528–543. Springer.

Zhang, R.; Li, W.; Wang, P.; Guan, C.; Fang, J.; Song, Y.; Yu, J.; Chen, B.; Xu, W.; and Yang, R. 2020. Autoremoval: automatic object removal for autonomous driving videos. In *Proceedings of the AAAI Conference on Artificial Intelligence*, volume 34, 12853–12861.

Zou, X.; Yang, L.; Liu, D.; and Lee, Y. J. 2021. Progressive temporal feature alignment network for video inpainting. In *Proceedings of the IEEE/CVF Conference on Computer Vision and Pattern Recognition*, 16448–16457.

Supplementary Material for "One-Shot Video Inpainting"

Sangjin Lee*, Suhwan Cho*, Sangyoun Lee

Yonsei University

1 Additional Study on Mask Prediction

As OSVI is a task to remove a designated object completely and fill in the missing regions, mask prediction is an important process for accurate OSVI. Here, we conduct an additional study on the mask prediction quality.

1.1 Quantitative Study

We evaluate the mask prediction quality of our method quantitatively. As the evaluation metrics, we adopt IoU and Recall. IoU is a general metric for evaluating segmentation performance, and can be obtained by the area of overlap over the area of union. Recall is a metric that calculates how much the ground truth region is sufficiently detected, and can be obtained by the area of overlap over the area of the ground truth. Considering OSVI is a task to completely remove a designated object, it will bring a severe error to the system if a tracker fails to track the object even in part. Therefore, unlike general segmentation tasks, Recall metric should be considered the major metric in OSVI.

In Table 1, our method is compared to state-of-the-art VOS methods quantitatively on the DAYT and BLDA datasets. Following previous settings, we adopt BMVOS (?), CFBI (?), and TBD (?) as the compared VOS solutions. Our method outperforms all other methods by a significantly margin. This is because of a joint learning of mask prediction and video completion modules, which can help each others' robust representation learning. It is also interesting that compared to other VOS methods, the predicted masks of our method have higher Recall scores compared to IoU scores. As the mask prediction module is trained considering the video completion module, it tends to predict the masks in a safe way (large masks), rather than a strict way (accurate masks).

1.2 Qualitative Study

In Figure 1, we also visualize the qualitative comparison of different model versions of our method. We compare the model without end-to-end training scheme (intentional disconnection of gradients between mask prediction module and video completion module), the model without encoder sharing (separate encoders for mask prediction and video completion), and the final model.

Compared the the model without end-to-end training, our final model outputs more accurate and stable masks. As described before, the mask prediction module tends to generate large masks instead of fine and accurate masks. This is because even a small lost of an object can bring a severe breakdown of a system. Our final model also shows better segmentation performance compared to the model that employs separate encoders for mask prediction module and video completion module. This demonstrates the effectiveness of a joint learning of mask prediction and video completion modules. As mask prediction and video completion share common complementary properties, sharing a single encoder enables a stable network training and strong feature representation learning.

*These authors contributed equally.

Table 1: Quantitative mask quality comparison of various models.

Version	DAYT		BLDA	
	IoU \uparrow	Recall \uparrow	IoU \uparrow	Recall \uparrow
Ours	81.6	91.1	80.4	89.2
BMVOS (?)	75.4 (-6.2)	84.2 (-6.9)	68.1 (-12.3)	77.0 (-12.2)
CFBI (?)	77.3 (-4.3)	82.4 (-8.7)	71.0 (-9.4)	76.2 (-13.0)
TBD (?)	79.5 (-2.1)	86.0 (-5.1)	77.8 (-2.6)	84.9 (-4.3)

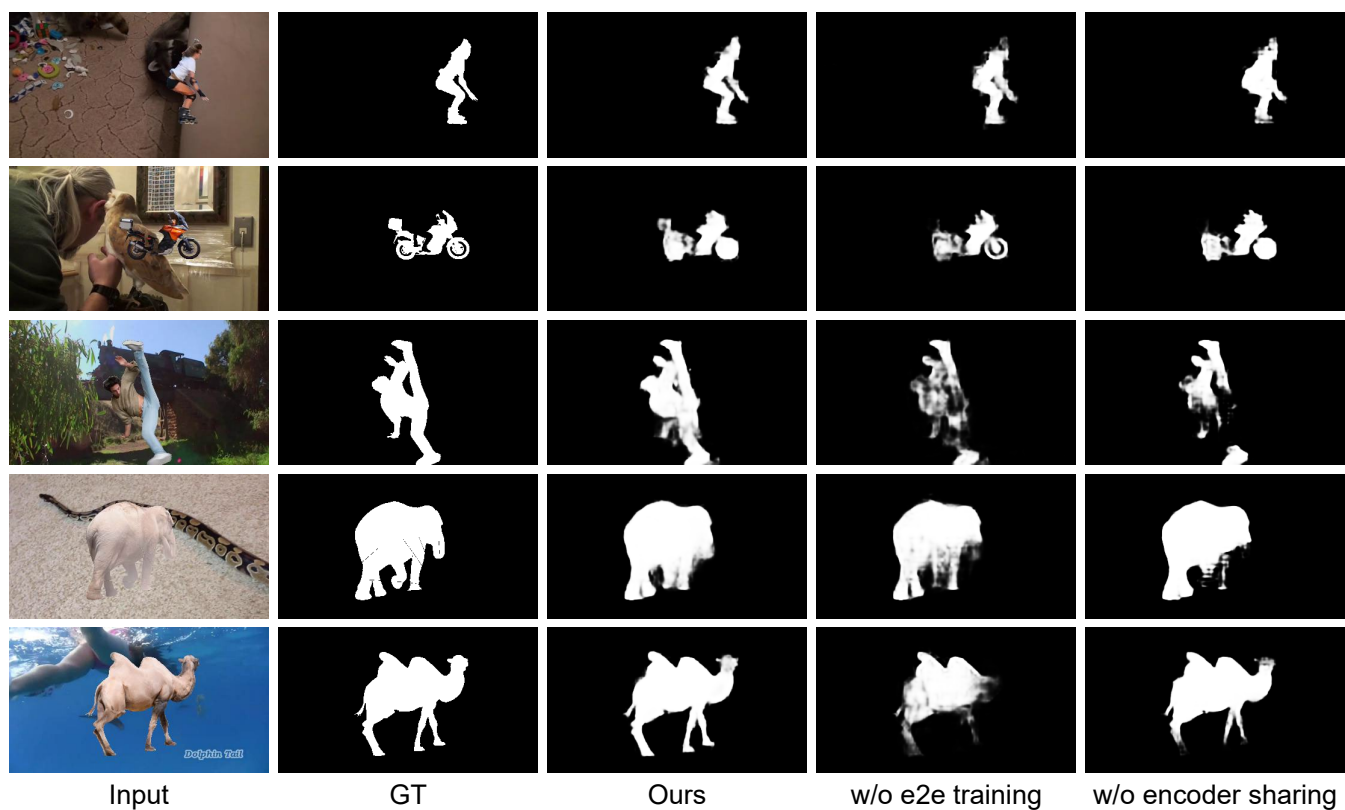


Figure 1: Qualitative mask comparison between various model versions.